19,05,11

Magnetocaloric properties of a ribbon sample of Heusler alloy $Ni_{45}Co_5Mn_{31}Al_{19}$: experimental and theoretical studies

© A.G. Gamzatov[1,2], V.V. Sokolovsky[1,2,3], A.B. Batdalov[1], A.M. Aliyev[1], D.-H. Kim[4], N.H. Yen[5], N.H. Dan[5], S.-C. Yu[6]

[1] Amirkhanov Institute of Physics, Dagestan Federal Research Center, Russian Academy of Sciences, Makhachkala, Russia
[2] National Research University of Technology „MiSiS“, Moscow, Russia
[3] Chelyabinsk State University, Chelyabinsk, Russia
[4] Department of Physics, Chungbuk National University, Cheongju, 28644 South Korea
[5] Institute of Materials Science, VAST, 18-Hoang Quoc Viet, Hanoi, Vietnam
[6] School of Natural Science, Ulsan National Institute of Science and Technology, Ulsan 44919, South Korea

E-mail: gamzatov_adler@mail.ru

Received September 28, 2022
Revised September 28, 2022
Accepted September 29, 2022

The results of experimental and theoretical studies of magnetocaloric properties of a ribbon sample of alloy $Ni_{45}Co_5Mn_{31}Al_{19}$ in the range of $T = 80-350$ K in magnetic fields of up to 8 T are given. This alloy demonstrates a first-order magnetostructural phase transition (MSPT) in the temperature range of 270 K, as well as a second-order transition — at the Curie temperature of 294 K. The magnetocaloric effect (MCE) was studied both by the direct method of magnetic field modulation in cyclic fields up to 8 T and by the classical extractive method. Field dependence of MCE have a different nature for first- and second-order phase transitions. A reverse MCE near MSPT is irreversible, i.e. the final sample temperature is 0.75 K below the initial one. Theoretical studies of magnetic properties and MCE of the studied sample were performed by *ab initio* calculations and Monte Carlo modeling. Theoretical temperature dependences of MCE are characterized by a similar interval of effect manifestation in the region of martensitic transformation and a narrower interval in the region of austenite Curie temperature as compared to the experiments, which is conditioned by the presence of a heterogeneous mixed state of austenite in the experimental sample. On the whole, theoretical data qualitatively and quantitatively reproduce the experimental dependences.

Keywords: magnetocaloric effect, cyclic fields, Heusler alloy, Monte Carlo method.

DOI: 10.21883/PSS.2022.12.54408.488

1. Introduction

Magnetic cooling based on the magnetocaloric effect (MCE) is a promising environmentally-friendly and energy-efficient cooling method. The MCE consists in an isothermal change of entropy (ΔS) or an adiabatic change of temperature (ΔT_{ad}) of a sample under application of an external magnetic field. Implementation of this technology requires that the material to have a large MCE value near room temperatures. Vivid representatives of magnetocaloric materials are Heusler alloys Ni–Mn–X (X — Al, Ga, In, Sn, Sb), which can change their magnetic properties upon a magnetostructural phase transition (MSPT), i.e. transform from low-magnetic martensite into ferromagnetic (FM) austenite, accompanied by a large reverse MCE. Composition can also be regulated to control the MSPT temperature to the necessary side [1–6].

It is known that operational efficiency of a MCE-based cooling machine can be enhanced by using materials of „reduced“ sizes,such as films, ribbons and microwires. These materials are interesting because of a higher surface area to volume ratio, i.e. a favorable geometry for heat transfer [2]. Moreover, ribbon materials are more workable, i.e. items of any configuration can be made from them.

The results of study of the influence of Al doping on the structure, magnetic properties and MCE of ribbon samples of $Ni_{50}Mn_{37-x}Al_xSn_{13}$ are given in [4,7–9]. Much data on MCE in ribbon samples of Heusler alloys in the available literature has been chiefly obtained by indirect methods based on measurement of isothermal magnetization curves [1–6]. However, such measurements for materials with structural transitions lead to rather large errors, since they neglect the entropy change due to a structural transition. In this context, direct MCE

measurements are preferable. We came across only several papers dedicated to the study of MCE of ribbon samples by the direct method [7–11]. This is due to the fact that direct studies of MCE in ribbon samples require special procedures, since the classical direct methods require bulkier samples. Recent studies of MCE [8] in a ribbon sample of $Ni_{50}Mn_{35}Al_2Sn_{13}$ in cyclic magnetic fields of 1.8 T by magnetic field modulation have shown than the value of reverse MCE depends on temperature scanning rate. The reason for this can be the kinetics of MSTP progress and relaxation processes. The higher the scanning rate, the higher the reverse effect value.

In the present paper we study (experimentally and theoretically) magnetic and magnetocaloric properties of a ribbon sample of Heusler alloy $Ni_{45}Co_5Mn_{31}Al_{19}$ obtained by quenching. The nature of magnetic phase transitions in the ribbon samples of $Ni_{50-x}Co_xMn_{50-y}Al_y$ ($x = 5$ and 10; $y = 17$, 18 and 19) was studied in a recent paper [12] which shows that Co doping greatly affects the magnetic phase transformation of materials. Partial substitution of Ni by Co in alloys leads to a significant change of magnetization under a martensitic transformation, which significantly increases the MCE [12–15]. Temperature of martensite transition to austenite decreases gradually, while the Curie temperature greatly increases with an increase of Co concentration. Substitution of Ni by Co enhances the magnetic exchange interactions and the ferromagnetic phase of alloys [16,17].

2. Samples and procedure

An alloy of nominal composition $Ni_{45}Co_5Mn_{31}Al_{19}$ was prepared using pure elements (99.9%) Ni, Co, Mn and Al by the method of arc melting in argon. Then we used the method of melt moulding for the making of ribbons from an alloy with the copper wheel tangential velocity of 40 m/s. Ribbon thickness and width are about 20 μm and 1.5 mm respectively [12].

The alloy structure was studied by the X-ray powder diffraction method (XRF). Magnetic properties were measured using a vibration magnetometer. MCE was studied both by the direct method and estimated by the Monte Carlo method (MC). The used direct method for measuring MCE in cyclic magnetic fields allows for measuring the adiabatic change of temperature ΔT_{ad} with a high accuracy ($\sim 10^{-3}$ K) in smaller samples (ribbons, films, nanowires etc.). It should be noted that measurements of ΔT_{ad} in small-size thin samples (films, ribbons) requires corrections to consider the ration of sample weight to weight of the thermocouple glued to the sample. Thickness of the thermocouple glued to the sample in our case is about 5–10 μm. A layered structure of (3–5 layers) of ribbons with a thermocouple between the layers was created to minimize the errors related to thermocouple weight.

The radiograph of the $Ni_{45}Co_5Mn_{31}Al_{19}$ ribbon, measured at room temperature, is shown in Fig. 1. The

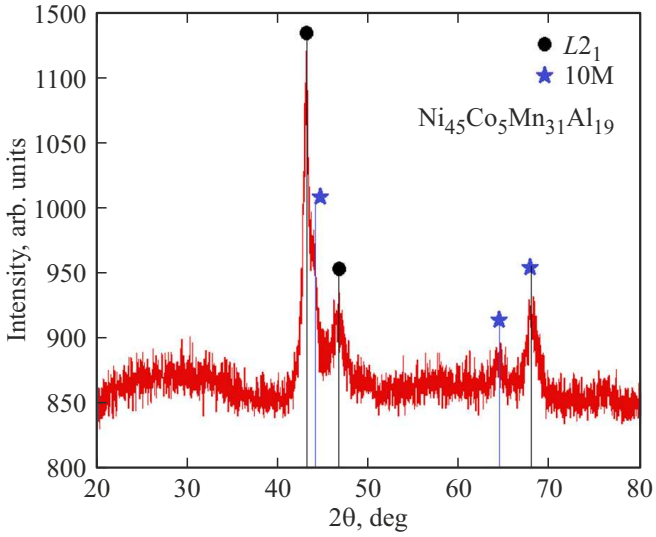

Figure 1. X-ray diffraction analysis of $Ni_{45}Co_5Mn_{31}Al_{19}$ alloy at room temperature.

structural analysis showed the presence of certain low-intensity peaks of XRD, corresponding to the martensitic phase 10M (space group: $Pmma$), in addition to the main phase related to the austenitic structure $L2_1$ (space group: $Fm3m$).

A theoretical study of magnetic and magnetocaloric properties of the studied compositions was performed within the framework of the density functional theory and MC modelling. The parameters of magnetic exchange interaction between Ni, Co and Mn atoms in the austenitic and martensitic phase were determined by ab initio methods, using the SPR-KKR software package [18] and GGA-PBE generalized gradients approximation as the exchange-correlation potential. The initial parameters of the cubic and tetragonal phases were determined from [19]. A coherent potential approximation was applied to form a non-stoichiometric composition $Ni_{45}Co_5Mn_{31}Al_{19}$. The thermodynamic characteristics were modelled using the MC method and a microscopic Blume–Emery–Griffiths–Heisenberg lattice model, taking into account the long-range exchange interactions between magnetic atoms, obtained by *ab initio* calculations [20–22]. The common Hamiltonian H consist of a magnetic (H_{mag}) and a lattice (H_{lat}) part, as well as a term of magnetoelastic interaction (H_{int}). It should be noted that a Potts model of q-states was chosen as a magnetic subsystem Hamiltonian in papers [20–22]. A Heisenberg Hamiltonian was considered in the present paper to describe magnetic interactions. Interactions between microdeformations in a structural subsystem were implemented within a Blume–Emery–Griffiths (BEG) Hamiltonian, which makes it possible to describe structural transformations from a cubic austenitic phase to a tetragonal martensitic phase with a thermal hysteresis. Complete information about the BEG Hamiltonian is given in [20–23].

Model parameters (in meV) and magnetic moments (in μ_B) for $Ni_{45}Co_5Mn_{31}Al_{19}$. Parameter U_1 — dimensionless constant

Phase	J	K	U_{ij}	U_1	μ_{Mn1}	μ_{Mn2}	μ_{Ni}	μ_{Co}
$c/a = 1$ (FM)	–	1.722	0.01	−0.4	3.411	3.615	0.429	1.126
$c/a = 1.25$ (FiM)	6.15	–	0.5	−0.4	3.349	−3.633	0.287	0.672

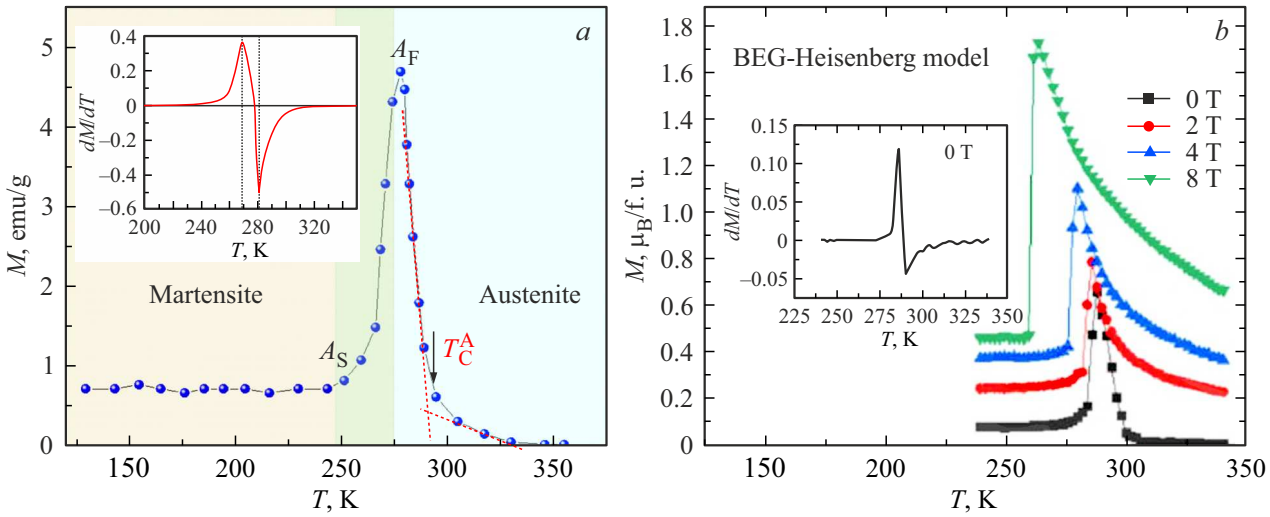

Figure 2. *a* — magnetization for sample heating vs. temperature at $H = 0.01$ T (heating mode). The inset shows dM/dT vs temperature; *b* — theoretical temperature dependences of magnetization in the magnetic fields of 0, 2, 4 and 8 T, obtained by Monte Carlo modeling. The inset shows dM/dT vs. temperature in the absence of a magnetic field.

MC modeling was performed on a three-dimensional lattice consisting of 11664 atoms (for Ni_2MnAl stoichiometry: 5832 atoms of Ni, 2916 atoms of Mn and Al). This lattice was obtained by ninefold translation of a sixteen-atom cell $L2_1$ in three directions ($9 \times 9 \times 9$). A non-stoichiometric composition was formed based on the nominal composition of the studied alloy ($Ni_{45}Co_5Mn_{31}Al_{19}$ or $Ni_{1.8}Co_{0.2}Mn_{1.24}Al_{0.76}$). Co atoms and redundant Mn atoms were located randomly at Ni and Al sites respectively. In order to implement the calculations for the ribbon sample, the boundary conditions were chosen cyclically in two directions, and in the third direction they were assumed to be open. A classical Metropolis algorism was used during modeling. The number of MC steps per one temperature value was $5 \cdot 10^5$. In order to attain thermal equilibrium in the system and to obtain equilibrium values of internal energy and order parameters, the first 10^4 MC steps were discarded. Thermodynamic quantities were averaged by 1225 configurations per each 400 MC steps.

As regards the selection of parameters of the model Hamiltonian, some of the parameters, such as magnetic interaction constants (J_{ij}) and magnetic moments (μ_i), were taken from the ab initio calculations. The other parameters, such as the constants of structural exchange interaction (J and K) and constants of magnetoelastic interaction (U_{ij}, U_1) were used as adjustment parameters for reproducing the temperature of martensitic transformation and experimental behavior of magnetization in different magnetic fields. It should be noted that the constants of magnetic interaction were considered up to the sixth coordination sphere and have a similar oscillating appearance given in [24]. The table gives the values of the parameters in the BEG−Heisenberg model.

According to [19], FM-ordering is profitable for the austenitic phase, while ferrimagnetic (FiM) ordering is profitable for the martensitic phase, i.e. magnetic moments of redundant Mn_2 atoms, located at the sites of Al atoms, are antiparallel to the magnetic moments of Mn_1, Ni and Co atoms. Here Mn_1 atoms are located at their regular sites.

3. Results and discussion

Fig. 2, *a* shows the temperature dependence of magnetization in the magnetic field of 100 Oe in the heating mode. When temperature decreases, sample magnetization increases abruptly due to sample's transition from the paramagnetic (PM) to the FM-state at the temperature of $T_C = 294$ K. Under further cooling, magnetization reaches the maximum at 277 K, and the decreases abruptly in the temperature range of 277 to 250 K, which is related to MSPT from the austenitic FM-phase to the martensitic antiferromagnetic one (AFM) [25]. In the temperature range of A_S to A_F, the austenitic and martensitic phases simultaneously exist in the sample; they have close transition temperatures, which considerably increases the magneti-

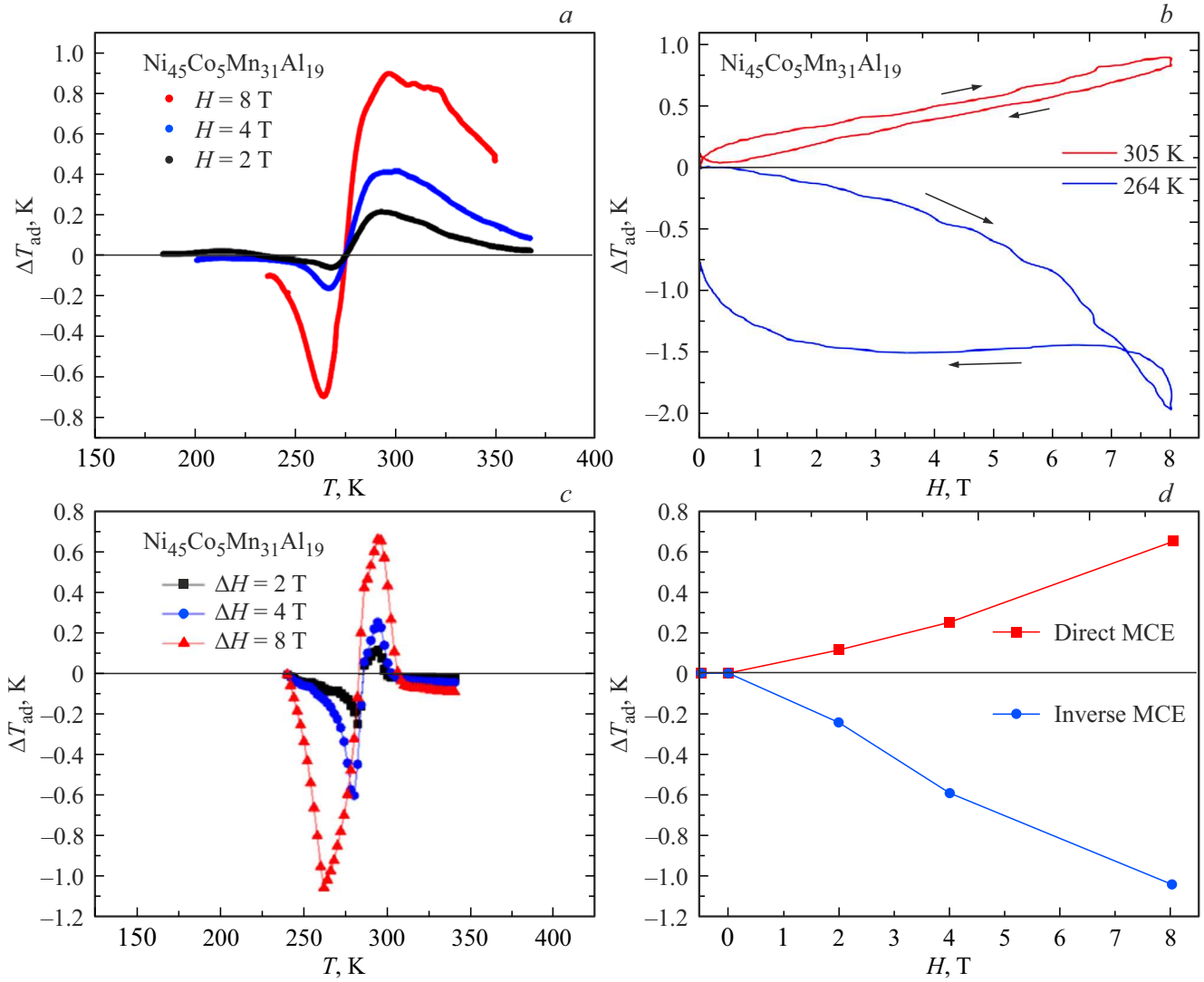

Figure 3. *a* — temperature dependence of MCE in the fields of 2, 4 and 8 T; *b* — field dependences of MCE at the first field activation; *c* — theoretical dependences of MCE in the fields of 2, 4 and 8 T obtained under heating; *d* — theoretical dependences of direct and reverse MCE as magnetic field functions obtained under heating (near the TS and MSTP).

zation value in this range. It should be noted that the two phase transitions are nearby: $T_C(\text{austenite}) = 294$ K, the start of a martensitic transformation $T_S = 270$ K. The dependence dM/dT, shown in the inset of Fig. 2, *a*, illustrate the aforesaid well.

Fig. 2, *b* shows the results of MC modeling of magnetization as temperature function for the studied compound in different magnetic fields up to 8 T. It is seen that the theoretical curve of magnetization reproduces well the experimental dependence shown in Fig. 2, *a*. According to the dM/dT derivative, theoretical temperatures of martensitic transformations and austenite Curie temperature are equal to 285 and 290 K, which is close to the experiment. The application of a magnetic field leads to a shift of martensitic transformation temperature T_M into the region of lower temperatures, which is related to stabilization of the austenitic S phase by a magnetic field. Thereat, the value of martensitic phase magnetization in both weak and in strong magnetic field is significantly lower than austenitic phase magnetization. Such behavior is due to a considerably competing interaction between Mn atoms in the martensitic phase. It should be noted that the described magnetization behavior is typical for Heusler alloy with an excess of Mn atoms.

Fig. 3, *a* shows the temperature dependence of MCE in the cyclic magnetic fields of 2, 4 and 8 T in the heating mode. The figure shows both a direct MCE ($\Delta T_{ad} > 0$) near T_C and an reverse MCE ($\Delta T_{ad} < 0$) near the MSTP temperature, the maximum values of ΔT_{ad} in the field of 8 T are equal to $+0.9$ K and -0.7 K respectively. The maximum temperature ΔT_{ad} near T_C does not depend on field intensity, while T_{max} near the MSTP shifts towards lower temperatures when the magnetic field increases.

A similar dependence $\Delta T_{ad}(H, T)$ near the MSTP was previously observed for the Ni−Mn−In alloy [26]. This behavior is explained by the fact that a magnetic field stabilizes the phase with the higher magnetization and causes a shift of the temperatures of martensitic transformation start towards low temperatures, and the effect maxima, as is known, are observed near the phase transformation temperatures.

Fig. 3, *b* shows the field dependence of MCE near the temperatures of the maxima of direct MCE (~ 305 K) and reverse (~ 264 K) MCE upon a single activation/deactivation of a magnetic field with the intensity of 8 T. As seen in the plot, the value of ΔT_{ad} near T_C reaches 0.9 K at 8 T, and upon field deactivation it returns, which a result of reversibility of the FM−PM phase transition. At $T = 264$ K, the value of reverse MCE in the field of 8 T in the field growth mode is equal to $\Delta T = -2$ K. An irreversible MSPT is observed upon field deactivation. Irreversibility of reverse MCE was considered in [27] and explained by a competition of direct and reverse MCE. It should be noted that the value of the reverse effect upon single activation of the magnetic field of 8 T is 2.2 times greater than the value obtained in the cyclic magnetic field of 8 T with the frequency of 0.13 Hz. This difference is due to the fact that the direct study of MCE in cyclic magnetic fields does not take into account the effects of the first activation.

MCE in the $Ni_{45}Co_5Mn_{31}Al_{19}$ ribbon alloy was estimated in [12] according to a change of magnetic entropy (ΔS_M) based on the magnetization isotherms. The maximum change of magnetic entropy at $\Delta H = 13.5$ kOe is about 2 and -1 J/kg · K for reverse and direct MCE respectively, which correlates well with the data of direct measurements upon a single activation of a magnetic field, where the maximum value of reverse effect is more than 2 times greater than the direct effect.

Let us consider the behavior of theoretical dependences of MCE (adiabatic change of temperature) as functions of temperature and magnetic field (see Fig. 3, *c, d*). In view of the close temperatures of martensitic transformation and austenite Curie temperature, it follows from Fig. 3, *c* that the reverse MCE, observed under a martensitic-austenitic transformation from the FiM- to FM-state, abruptly changes for the direct MCE which occurs in the region of the FM−PM-transition of the austenitic phase. The calculations show that the greatest MCE is observed in the region of MSTP, which pertains to the first-order phase transition. On the contrary, according to the experimental data, the greatest value of MCE is implemented in the region of the austenite Curie temperature (see Fig. 3, *a*). This difference can be explained by a heterogeneous mixed state in the region of a structural transformation due to a competition of volume ratios of the martensitic and austenitic phases. A magnetic field growth intensifies both the direct and reverse MCE. On the whole, qualitative and quantitative agreement between the theoretical and experimental MCE values can be observed.

4. Conclusion

Temperature dependences of magnetization and MCE for a fast-quenched ribbon sample of $Ni_{45}Co_5Mn_{31}Al_{19}$ in the temperature range of 150−350 K and in magnetic fields up to 8 T were studied. The results of the study of MCE upon a single activation of magnetic field show that the reverse effect value is equal to $\Delta T \ll -2$ K in the field of 8 T. The reverse effect value in the cyclic magnetic field of 8 T is equal to -0.9 K. The afield dependence of MCE near T_C is linear, while an irreversible MCE is observed near the MSTP. Similar results were obtained within the framework of MC modeling. The direct and reverse MCE value varies almost linearly with an increase of magnetic field intensity. However, the effect of the first activation cannot be recorded within the framework of the proposed model due to its imperfection. Moreover, the theoretical curves of MCE are characterized by a narrow interval of effect manifestation in the region of the Curie temperature as compared to the experiment, which is conditioned by the presence of a heterogeneous mixed state of austenite in the experimental sample due to a competition of volume ratios of the martensitic and austenitic phases. Nevertheless, the obtained temperature dependences of magnetization and MCE reproduce the experimental data qualitatively and quantitatively. Temperature behavior of magnetization in different fields has also been predicted within the framework of the proposed theoretical approach; this behavior demonstrates a shift of the sudden change of magnetization to the low temperature region due to a shift of the structural transition temperature by a magnetic field.

On the whole, we can assume that a combination of experimental and theoretical approaches will help improve the understanding of thermophysical processes accountable for MCE manifestation in Heusler alloys with a related magnetostructural transition.

Acknowledgments

The authors would like to thank Sh.K. Khizriyeva for support and A.T. Kadyrbardeeva for help in the experiments.

Funding

The study was funded by a grant of the Russian Science Foundation No. 22-19-00610.

Conflict of interest

The authors declare that they have no conflict of interest.

References

[1] F-x. Hu, B-g. Shen, J-r. Sun, G-h. Wu. Phys. Rev. B **64**, 132412 (2001).
[2] V.V. Khovaylo, V.V. Rodionova, S.N. Shevyrtalov, V. Novosad. Phys. Status Solidi B 1 (2014).

[3] L. González-Legarreta, W.O. Rosa, J. García, M. Ipatov, M. Nazmunnahar, L. Escoda, J.J. Suñol, V.M. Prida, R.L. Sommer, J. González, M. Leoni, B. Hernando. J. Alloys Comp. **582**, 588 (2014).
[4] H.Y. Nguyen, T.M. Nguyen, M.Q. Vu, T.T. Pham, D.T. Tran, H.D. Nguyen, L.T. Nguyen, H.H. Nguyen, V.V. Koledov, A. Kamantsev, A. Mashirov. Adv. Nat. Sci.: Nanosci. Nanotechnology **9**, 025007 (2018).
[5] W. Guan, Q.R. Liu, B. Gao, S.Yang, Y. Wang, M.W. Xu, Z.B. Sun, X.P. Song. J. Appl. Phys. **109**, 07A903 (2011).
[6] H.C. Xuan, K.X. Xie, D.H. Wang, Z.D. Han, C.L. Zhang, B.X. Gu, Y.W. Du. Appl. Phys. Lett. **92**, 242506 (2008).
[7] A.G. Gamzatov, A.B. Batdalov, Sh.K. Khizriev, A.M. Aliev, L.N. Khanov, N.H. Yen, N.H. Dan, H. Zhou, S. Yu, D. Kim. J. Alloys Comp. **842**, 155783 (2020).
[8] A.G. Gamzatov, A.M. Aliev, A.B. Batdalov, Sh.K. Khizriev, D.A. Kuzmin, A.P. Kamantsev, D.-H. Kim, N.H. Yen, N.H. Dan, S.-C. Yu. J. Mater. Sci. **56**, 15397 (2021).
[9] Sh.K. Khizriev, A.G. Gamzatov, A. B. Batdalov, A.M. Aliev, L.N. Khanov, D.-H. Kim, S.-C. Yu, N.H. Yen, N.H. Dan. Phys. Solid State **62**, 1280 (2020).
[10] A.M. Aliev, A.B. Batdalov, I.K. Kamilov, V.V. Koledov, V.G. Shavrov, V.D. Buchelnikov, J. García, V.M. Prida, B. Hernando. Appl. Phys. Lett. **97**, 212505 (2010).
[11] F. Cugini, D. Orsi, E. Brück, M. Solzi. Appl. Phys. Lett. **113**, 232405 (2018).
[12] Y. Nguyen, M. Nguyen, Q. Vu, T. Pham, V.V. Koledov, A. Kamantsev, A. Mashirov, T. Tran, H. Kieu, Y. Seong, D. Nguyen. EPJ Web Conf. **185**, 05001 (2018).
[13] G.P. Felcher, J.W. Cable, M.K. Wilkinsonm. Phys. Chem. Solids **24**, 1663 (1963).
[14] F. Gejima, Y. Sutou, R. Kainuma, K. Ishida. Metallurg. Mater. Transact. A **30**, 2721 (1999).
[15] H.C. Xuan, F.H. Chen, P.D. Han, D.H. Wang, Y.W. Du. Intermetallic **47**, 31 (2014).
[16] M.V. Lyange, E.S. Barmina, V.V. Khovaylo. Mater. Sci. Foundations **81**, 232 (2015).
[17] C. Liu, W. Zhang, Z. Qian, Z. Hu, Q. Zhao, Y. Sui, W. Su, M. Zhang, Z. Liu, G. Liu, G. Wu. J. Alloys Comp. **433**, 37 (2007).
[18] H. Ebert, D. Ködderitzsch, J. Minár. Rep. Prog. Phys. **74**, 096501 (2011).
[19] M.V. Lyange, V.V. Sokolovskiy, S.V. Taskaev, D.Yu. Karpenkov, A.V. Bogach, M.V. Zheleznyi, I.V. Shchetinin, V.V. Khovaylo, V.D. Buchelnikov. Intermetallics **102**, 132 (2018).
[20] V.D. Buchelnikov, V.V. Sokolovskiy, H.C. Herper, H. Ebert, M.E. Gruner, S.V. Taskaev, V.V. Khovaylo, A. Hucht, A. Dannenberg, M. Ogura, H. Akai, M. Acet, P. Entel. Phys. Rev. B **81**, 094411 (2010).
[21] D. Comtesse, M.E. Gruner, M. Ogura, V.V. Sokolovskiy, V.D. Buchelnikov, A. Grünebohm, R. Arróyave, N. Singh, T. Gottschall, O. Gutfleisch, V.A. Chernenko, F. Albertini, S. Fähler, P. Entel. Phys. Rev. B **89**, 184403 (2014).
[22] V. Sokolovskiy, A. Grünebohm, V. Buchelnikov, P. Entel. Entropy **16**, 4992 (2014).
[23] T. Castán, E. Vives, P.-A. Lindgard. Phys. Rev. B **60**, 7071 (1999).
[24] V.V. Sokolovskiy, O. Miroshkina, M. Zagrebin, V. Buchelnikov. J. Appl. Phys. **127**, 163901 (2020).
[25] C. Jing, J. Chen, Z. Li, Y. Qiao, B. Kang, S. Cao, J. Zhang. J. Alloys Comp. **475**, 1 (2009).
[26] A.B. Batdalov, L.N. Khanov, A.V. Mashirov, V.V. Koledov, A.M. Aliev. J. Appl. Phys. **129**, 123901 (2021).
[27] V.V. Khovaylo, K.P. Skokov, O. Gutfleisch, H. Miki, R. Kainuma, T. Kanomata. Appl. Phys. Lett. **97**, 052503 (2010).